A Search for Lepton Flavor Violating Decays of the Higgs Boson and a Measurement of W Boson Production using the CMS Detector at the LHC

by

Aaron Levine

A dissertation submitted in partial fulfillment of
the requirements for the degree of

Doctor of Philosophy
(Physics)

at the
University of Wisconsin – Madison
2016

Defended on
Dissertation approved by the following members of the Final Oral Committee:
Sridhara Dasu · Professor of Physics
Wesley Smith · Professor of Physics
Other Member · Professor of Physics
Other Member · Professor of Physics
Other Member · Professor of Other Department

Abstract

Abstract Goes Here

Acknowledgements

This is where any acknowledgements would go.

Contents

List of Figures

List of Tables

Chapter 1

Theoretical Motivation

1.1 The Standard Model

Our knowledge of particle interactions is summarized in a theory called the Standard Model. The theoretical framework of the Standard Model was developed over the course of the 20th century as more and more fundamental particles and forces were discovered and studied. The Standard Model is not without its flaws. It is a phenomenological theory that contains many free parameters, such as the masses of the particles, that can only be determined from experiment. It also fails to include the gravitational interactions, and thus only describes three of the four fundamental forces. The ad hoc design of the Standard Model and the lack of unification provides a strong motivation for particle physicists to search for a more profound, comprehensive theory. The current state of particles physics takes a two pronged approach, with physicists making precision measurements of the Standard Model and searching for physics beyond the Standard Model. The goal is to measure the parameters of the Standard Model while searching for the theory's replacement.

Elementary Particles

The fundamental particles in the Standard Model are summarized in figure. The fundamental particles consist of fermions and bosons. The fermions are particles that have half integer spin, and the bosons have integer spin. Spin is the intrinsic quantized angular momentum of a particle. The bosons mediate the fundamental forces and provide mass. They will be discussed further in Section 1.1.2 and Section 1.1.3. The fermions consist of the quarks, leptons, and neutrinos.

There are three generations of quarks, with two flavors in each generation. Each quark

generation consists of a quark with +2/3 of an electron charge (+2/3e) and a quark with -1/3 of an electron charge (-1/3e). Quarks also have a property known as "color." There are three possible colors for each quark: red, green, or blue. The concept of color is important for understanding the strong nuclear force, as discussed in Section 1.1.2. As shown in figure 1.1 the masses of the quarks vary significantly from one generation to the next.

Free quarks have never been observed in nature. Only color neutral combinations of quarks have been observed. For example, a red, green, or blue quark can form a stable state with a corresponding antiquark. This state is known as a meson. The baryons consists of three quarks, one of each color. The proton (uud), and the neutron (udd), are both baryons. Matter than is composed of quarks is called hadronic matter.

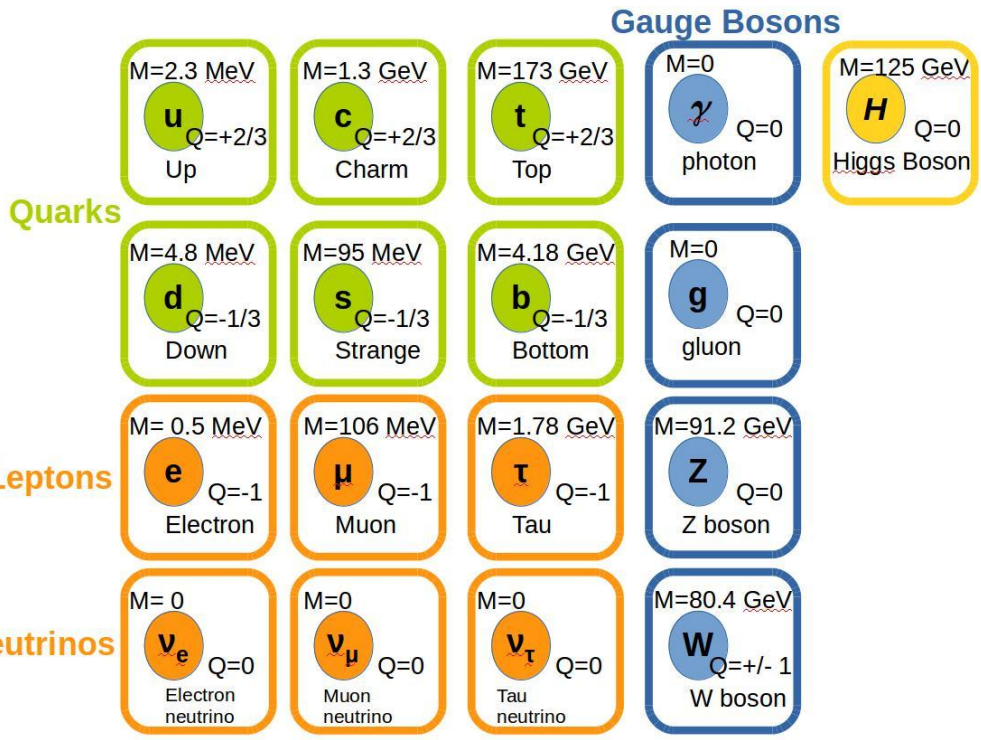

Figure 1.1: The fundamental particles of the Standard Model. Charges are expressed in units of electron charge.[17]

There are three generations of leptons, each with a neutrino pair. The electron is extremely light and does not decay, but the muon and the tau are heavier and have lifetimes on the order of $10^{-6}s$ and $10^{-15}s$ respectively[17]. The mechanisms for lepton decay will be discussed in Section 1.1.2 . In the Standard Model, there is a conserved quantity known as the lepton number. Each

lepton/neutrino pair, such as an e and an ν_e each will have an electron lepton number of 1, and the corresponding antiparticle pair will have a lepton number of -1. Figure 1.2 gives an example of a decay that conserves lepton number. In the initial state only the tau exists and the tau lepton number of the system is one while the muon and electron lepton numbers of the system are 0. The decay produces a tau neutrino which also has a tau lepton number of one along with an electron and an antielectron neutrino, which have electron lepton numbers of one and negative one, respectively. So the final state also has a tau lepton number of one. Also note that lepton number and flavor are conserved at each vertex.

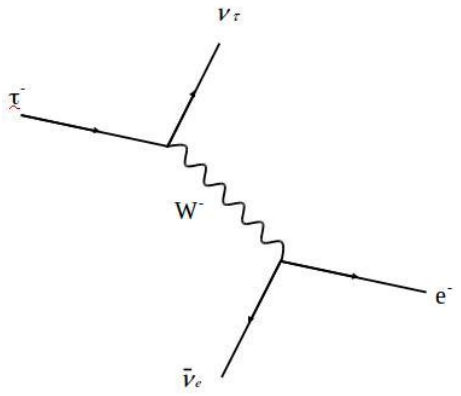

Figure 1.2: Decay of the tau lepton, as mediated by the W boson. The W boson is discussed further in Section 1.1.2.

Elementary Forces

Force	Relative Strength	Mediator
Strong	1	Gluon
Electromagnetic	10^{-3}	Photon
Weak	10^{-11}	W,Z Boson

Table 1.1: Fundamental forces of the Standard Model[14].

The fundamental forces of the Standard Model are shown in Table 1.1. Note that gravity is not included in the table. Gravity is not contained in the standard model and has a strength on the order of 10^{-30} [7] relative to the weak nuclear force. It plays a negligible role in high energy physics.

The theory of the electromagnetic for is know as quantum electrodynamics (QED). The Electromagnetic force is mediated by the photon. The photon is a spin 0 massless particle. Two

examples of electromagnetic interactions are show in figure 1.3 . The photon only interacts with particles that carry charge.

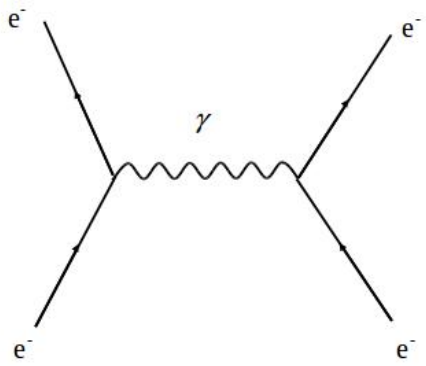

Figure 1.3: A photon mediating scattering between two electrons

The weak nuclear force is mediated by the W and Z bosons. The Z boson is a neutral spin 1 particle. It decays into pairs of quarks, leptons, or neutrinos. The W boson is a charged spin 1 particle. It has the special property of changing flavors of quarks and leptons. For example, the W boson can mediate the decay of a tau to an electron. This is illustrated in figure 1.2. Note that lepton number is still conserved in these types of interactions.

The theory of the strong nuclear force is known as quantum chromodynamics (QCD). The strong nuclear force is mediated by the gluon. Each gluon is a color doublet, with a corresponding color and anticolor. For example, a gluon could be red and antigreen, or blue and antired, et cetera. Gluons only interact with particles that share one of their color charges. Therefore, the quarks are the only particles involved in strong interactions. Virtual gluons can self interact which increases the strength of the color charge surrounding a quark. At small distances scales the virtual gluon cloud is penetrated and the effective color charge decreases. This effect is known as asymptotic freedom. [14] At larger distances, as a quark antiquark pair move apart from each other, the increase in potential energy allows new quark antiquark pairs to be created from the vacuum. The new quarks will be bound to the initial quarks by the strong nuclear force, which is why free quarks have never been observed.

The Higgs Boson

In classical physics, the equations of motion of a system are governed by the Lagrangian. The Lagrangian is defined as $L = T - V$ where T is the kinetic energy and V is the potential energy. In the Standard Model, we can also define a Lagrangian that governs all particle interactions[14] However, when mass terms for W and Z bosons are added to the Lagrangian, the Standard Model breaks down. Loops formed by W and Z bosons contribute infinities to Standard Model calculations that cannot be removed. This means that the Standard Model becomes unrenormalizable.

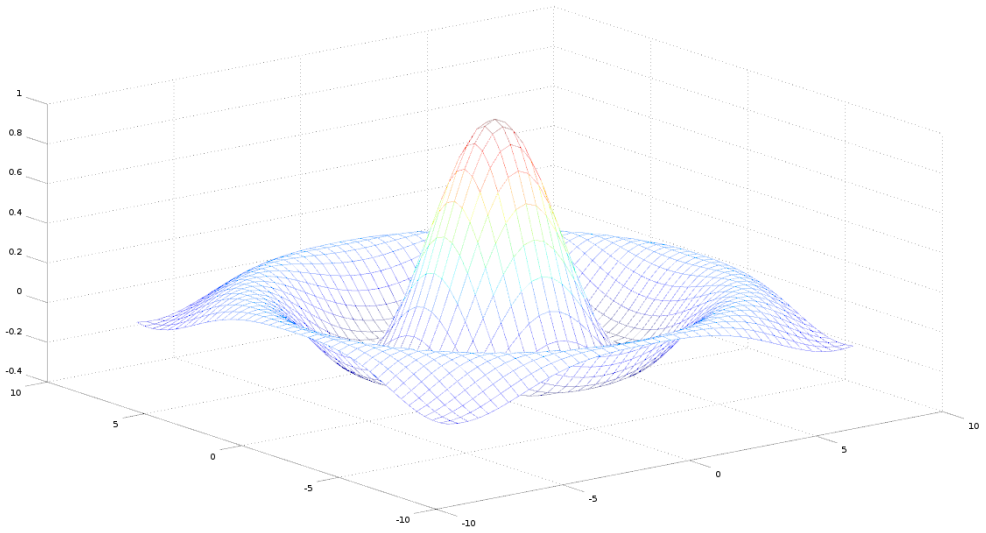

Figure 1.4: The potential of the Higgs Field. Note the nonzero minima.

To resolve this, we introduce a field with a potential shown in figure 1.4. This potential has a minimum that is not at the origin of the coordinate system. We can break the symmetry by shifting our reference point to the minimum of the potential and expanding for small deviations about the minimum. When this shift is introduced to the Lagrangian, it results in mass terms appearing for the W and Z bosons, the quarks and leptons, and a mass term for the particle associated with the field itself. That particle is known as the Higgs Boson. In addition to providing the theoretical framework to add mass terms to the Lagrangian, the Higgs Boson couples to every massive particle in the Standard Model. The couplings of the Higgs to the W and Z bosons cancel out the infinities mentioned earlier.[14] Thus, the field that naturally gives rise to masses in the Standard Model also cancels out the divergences that prevented us from simply placing mass terms in the Lagrangian to begin with. A Higgs Boson with a mass of 125 GeV was discovered at CERN on July 4 2012. [17]

1.2 Beyond the Standard Model

As mentioned in section 1.0 the Standard Model requires many free parameters determined by experiment and fails to unify gravity with the other four fundamental forces. Additionally, it fails to account for neutrino oscillations[13][1][2] and it doesn't address the hierarchy problem. [6] A more fundamental theory must exist, and the recently discovered Higgs boson provides a rich environment for probing the existence of such a theory. Many proposed theories such as Randall-Sundrum models [18] or Two Higgs Doublet models [9] predict a Higgs boson with couplings that violate lepton flavor conservation. The strength of Higgs couplings are proportional to the masses of the particles involved, so the most logical place to start a search for lepton flavor violation would be a Higgs boson coupling directly to the two heaviest leptons: a muon and a tau.

There have been no direct searches for $H \to \mu\tau$ prior to the result contained in this dissertation. Null searches for $\tau \to \mu\gamma$ constrain the branching fraction for $H \to \mu\tau$ to $\mathcal{O}(10\%)$.[15]

Chapter 2

LHC Phenomenology

2.1 Proton-Proton Collisions

2.2 W Boson Production: Mention prior results

2.3 Higgs Boson Production

Chapter 3

Experimental Design: The Headings below are self explanatory

3.1 LHC

3.2 CMS

Overview

Tracker

ECAL

HCAL

Muon System

Trigger

Chapter 4

Event Simulation

Particle interactions at CMS are very difficult to model. The strong nuclear force plays a very large role in proton-antiproton collisions, but calculations involving QCD are notoriously difficult. At short distances on the order of a femtometer, we can define the momentum scale Q to be much greater than Λ_{QCD}. This means that the effects of QCD can be calculated perturbatively (pQCD), which means that high order terms can be neglected and accurate predictions can be made. However, at Λ_{QCD} there are enormous amounts of soft radiation whose effects would be overwhelming to calculate by hand.

Additionally, the interactions of the collision products with the the detector components are very complicated and are effectively impossible to model by hand. Accurate models of physical processes at CMS are vital for testing existing theories and searching for new ones, so the difficulty of modelling these processes presents a significant challenge for CMS and for particle physics in general.

4.1 Monte Carlo Event Generation

Physical processes at CMS are simulated using a class of software called Monte Carlo generators. These programs are named after the famous casino because Monte Carlo software leans heavily on random number generation to simulate the kinematic distribution and decay chains of the event products. When using Monte Carlo software to simulate collisions, the user must specify the center of mass energy, the initial colliding particles, and the desired final products. Additional parameters can be defined by the user, such as the hadronization scale discussed in section 4.1. The three

main components of Monte Carlo simulation are matrix element computation, parton showering, and hadronization.

Matrix Elements

Once the initial and final state particles are specified, a series of Feynman diagrams are created. By using Feynman rules as discussed in chapter 1 and averaging over helicity and color, production amplitudes are computed for the process. However, this calculation provides only a very basic picture of the event and neglects soft radiation at the pQCD scale.

Parton Showering

As discussed in chapter 2, in high energy collisions protons can be modeled as collections of partons where the partons are pointlike particles carrying a particular fraction of the proton's momentum. Parton distribution functions, as discussed in chapter 2, provide a model of how the protons will interact in a collision.

After the collision, Sudakov Form Factors[17] are computed, which represent the probablity of a parton splitting into multiple partons. A low momentum bound for splitting is defined, and all partons above this threshold are randomly split in accordance with the probability of splitting. Color is properly accounted for at each vertex. Parton showers simulate QCD radiation emitted by quarks in the form of gluons, or a gluon splitting into two quarks.

At this point it is necessary to reconcile the matrix element computation, which represents high energy hard scattering, with parton showers, which model soft radiation. Two methods are available. The matrix element and parton shower method (ME+PS) and the next to leading order and parton shower method (NLO+PS)[17]. In the ME+PS method, matrix elements are computed for the fundamental process with the addition of n partons. The additional partons are required to be separated by a specified transverse momentum threshold. The momentum threshold is chosen to be at the upper limit of pQCD. In this way, the event can be computed accurately at large angle via matrix element methods, and then parton showering algorithms can be applied to the additional partons in the event. The ME+PS method is good for simulating events with many hard jets that are well separated. These kind of jets are simulated much better with tree level computations rather than lower energy pQCD parton showering. The next to leading order and parton shower method (NLO+PS) extends to parton shower method to next to leading order to QCD.

Hadronization

After parton showering, the event consists of the hard final products and many soft partons. At this point, the partons must transform into color singlet final state hadrons. One way to the this is the Lund string model. In this model, quark and anti-quark pairs are connected by color "strings" with a potential $V(r) = \kappa r$ As the quarks and anti-quarks move apart, the string breaks and an additional quark anti-quark pair or a gluon is created. The p_T of the quark or anti-quark is $< p_T^2 >= \kappa/\pi$ and the Lund fragmentation function[17] defines the fraction of the longitudinal momentum of the endpoint particle that is imparted to its recently produced neighbor. In this fashion, the kinematic variables of the produced hadrons are known, and the shower continues until an energy scale cutoff is reached. This process is depicted in figure 4.1

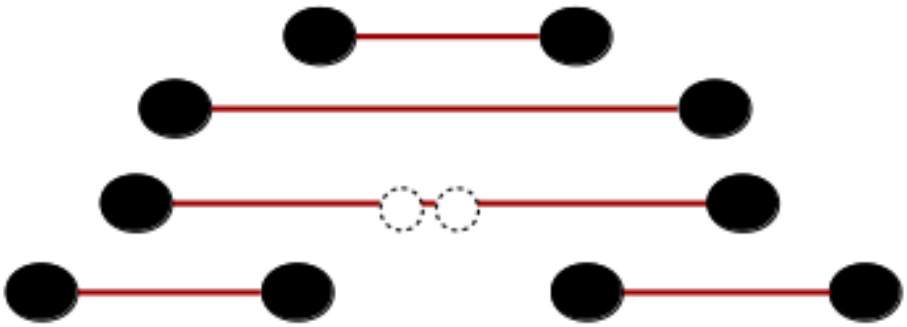

Figure 4.1: An illustration of the Lund string model. As the quark/anti-quark pair move further apart, the increase in potential energy creates an additional quark/anti-quark pair.

Monte Carlo Generator Software

A variety of different Monte Carlo generators are used at CMS. MADGRAPH [5] is used to compute leading order matrix elements. Its output is piped into PYTHIA[20], which models parton showers and hadronization using the Lund String Model. The combination of MADGRAPH and PYTHIA is an example of the ME+PS technique. Alternatively, NLO matrix elements can be computed with aMC@NLO[5] or POWHEG[3, 12, 16]. Parton showers and hadronization are once again simulated with pythia. This is an example of the NLO+PS technique.After hadronization, some heavy states may still need to decay. The τ lepton is too short lived to be directly observed in the detector, so any Monte Carlo simulation must decay the τ further. TAUOLA [22] is interfaced with

PYTHIA to provide an accurate view of τ decay by taking into account τ helicity and polarization.

4.2 Detector Simulation

After the simulation of the physical process, complete with parton showering and hadronization, it is necessary to model the interactions of the finale state particles with the CMS detector. This is done using GEANT4[4]. First, an accurate model of the CMS detector must be built in GEANT4, defining both the geometry and material components of the detector. The simulation is then carried out in two steps: tracking and detector response. The tracking step simulates the passage of particles through matter, modelling the energy lost based on the particles and the detector material. The next step is to model the detector response. This will simulate the signal that each event will create. Once the detector simulation is complete, we will have a very good idea of what a particular physical process at CMS will look like from the point of view of the detector. Now the challenge is the reconstruct the constituents of the event from the detector response, which is discussed in the next chapter.

Chapter 5

Event Reconstruction: Discuss how physics objects are reconstructed from detector deposits or lack thereof

5.1 Particle Flow

5.2 Electrons

5.3 Muons

5.4 Hadrons

5.5 Jets

5.6 MET

Chapter 6

Analysis Methods: Summarize W+Jets and LFV Higgs ANs

6.1 Background Estimation

Monte Carlo Samples Used: This section will simply list the Monte Carlo samples used, in contrast with the Monte Carlo Generation section which will list the different Monte Carlo generator techniques.

QCD Estimation

Tau Embedding

Fake Rate Method

6.2 Selection Optimization

W+Jets

LFV Higgs

6.3 Systematic Uncertainties

W+Jets

LFV Higgs

Chapter 7

Results

7.1 LFV Higgs

Statistical Methods

Maximum Likelihood Fit

After selecting events which pass the signal region selections and defining sources of systematic uncertainty, the next step is to fit the backgrounds to the data. This is done via a binned maximum likelihood fit.[8][10] We assume that the number of events in each bin follows a Poisson distribution, defined as $P(n_i|\mu_i) = \frac{\mu_i^{n_i} e^{-\mu_i}}{n_i!}$, where n_i is the number of events in the i^{th} bin and μ_i is the number of Monte Carlo events in each bin.

We then define the likelihood L as $L = \prod P(n_i|\mu_i)$. The goal of the fit is to determine the μ_i that maximizes the likelihood. This procedure is complicated by the addition of the systematic uncertainties, which are treated as nuisance parameters. For example, the luminosity uncertainty introduces a 2.3% uncertainty. To account for this, each term in the likelihood expression is multiplied by a log-normal distribution. The log-normal distribution is used instead of the Gaussian distribution to prevent the parameter from becoming negative. The lognormal distribution is defined: $N(\mu, \sigma) = \frac{1}{x\sigma\sqrt{2\pi}} e^{-\frac{(\log x - \mu)^2}{2\sigma^2}}$. Shape uncertainties, like the jet energy scale and tau energy scale systematics, are represented by Gaussian distributions. For the j^{th} sample in the i^{th} bin we can write: $\epsilon_{ji} = \epsilon^0_{ji} + f\frac{\epsilon^+_{ji} - \epsilon^-_{ji}}{2}$. Here, ϵ^0_{ji} is the efficiency before the shift, ϵ^+_{ji} is the efficiency after the scale shift up, and ϵ^-_{ji} is the efficiency after the scale shift down. The morphing parameter f has a gaussian distribution. We can interpolate quadratically for $|f| < 1$ and write

$\epsilon_{ji} = \frac{f(f-1)}{2}\epsilon^{-}_{ji} - (f-1)(f+1)\epsilon^{0}_{ji} + \frac{f(f+1}{2}\epsilon^{+}_{ji}$ This term is then added as an additional factor in the maximum likelihood formula.

The postfit histograms are shown in Figure 7.1.

Maximum Likelihood Limits

After computing the expected LFV signal branching ratios, the next step is to determine the statistical significance of the result. The profile likelihood $\lambda(\mu)$ is defined as $\lambda(\mu) = \frac{L(\mu,\hat{\hat{\theta}})}{L(\hat{\mu},\hat{\theta})}$ where μ is the hypothesized signal strength defined by $\mu = 0$ as the background hypothesis and $\mu = 1$ the signal hypothesis. [11] The nuisance parameters are represented by θ. The denominator is the maximum value of the likelihood function, where $\hat{\mu}$ and $\hat{\theta}$ take their values that maximize the likelihood. The numerator is a likelihood as a function of μ, where $\hat{\hat{\theta}}$ maximizes the likelihood for a given μ. The profile likelihood can range between 0 and 1. We define our test statistic as $t_\mu = -2\ln\lambda\mu$. The probability distribution of this test statistic is given by $t_\mu = \frac{\mu-\hat{\mu}}{\sigma^2} + \mathcal{O}(\frac{1}{\sqrt{N}})$. [21] Here σ is related to the variance of all the nuisance parameters. We can make the asymptotic approximation that the second term goes to zero as $N \to \infty$. This is known as the asymptotic approximation.

Note that the test statistic is zero for total agreement between the hypothesis and the data and decreases as the data differs more and more from the hypothesis. The probability to observe a given hypothesis μ is defined by $p_\mu = \int_{\mu_{obs}}^{\infty} -2ln\lambda(\mu)$. The p-value is defined as $p_{\mu=0}$ and is the probability to exclude the background hypothesis. If $p < \alpha$ then we can consider the background hypothesis to be excluded. In high energy physics we define α as 2.87×10^{-7}. It is customary to express the in terms of standard deviations from the mean, assuming a Gaussian probability distribution function (PDF). For a p-value of 2.87×10^{-7} the significance is 5σ.

It is customary to use 95% confidence intervals when setting limits. If $p_\mu < 5\%$ then the hypothesis where the signal strength is μ can be excluded at 95% confidence. However, if the background is very small or fluctuates downward, it is possible to exclude a signal that the analysis is not sensitive to. This can be avoided by using the CL_s method. [19] The p-value for the CL_s method is defined by dividing the p-value for the signal hypothesis by the probability for excluding the background, which is $(1 - p_{\mu=0})$.

It is useful to compare the observed limit with the expected limit. The expected limit is determined by generating an Asimov dataset [11] which is consistent with the background hypothesis. By definition, the Asimov dataset will produce postfit nuisance parameters that are identical to their

expected values. The expected limit is a useful statistic that measures the exclusion power of an analysis. For example, if the expected limit is significantly greater than the signal hypothesis, then the analysis does not have the statistical power to investigate the signal region.

8 TeV Results

The M_{col} distributions after the fit for signal and background contributions are shown in Fig. 7.1 and the event yields in the mass range $100 < M_{\text{col}} < 150$GeV are shown in Table 7.1. The different channels and categories are combined to set a 95% CL_s upper limit on the branching fraction of LFV Higgs decay in the $\mu\tau$ channel, $B(H \to \mu\tau)$.

Table 7.1: Event yields in the signal region, $100 < M_{\text{col}} < 150$GeV after fitting for signal and background. The expected contributions are normalized to an integrated luminosity of 19.7 fb^{-1}. The LFV Higgs boson signal is the expected yield for $B(H \to \mu\tau) = 0.84\%$ with the SM Higgs boson cross section.

Sample	$H \to \mu\tau_h$			$H \to \mu\tau_e$		
	0-Jet	1-Jet	2-Jets	0-Jet	1-Jet	2-Jets
misidentified leptons	1770 ± 530	377 ± 114	1.8 ± 1.0	42 ± 17	16 ± 7	1.1 ± 0.7
$Z \to \tau\tau$	187 ± 10	59 ± 4	0.4 ± 0.2	65 ± 3	39 ± 2	1.3 ± 0.2
ZZ, WW	46 ± 8	15 ± 3	0.2 ± 0.2	41 ± 7	22 ± 4	0.7 ± 0.2
$W\gamma$	NA	NA	NA	2 ± 2	2 ± 2	NA
$Z \to ee$ or $\mu\mu$	110 ± 23	20 ± 7	0.1 ± 0.1	1.6 ± 0.7	1.8 ± 0.8	NA
$t\bar{t}$	2.2 ± 0.6	24 ± 3	0.9 ± 0.5	4.8 ± 0.7	30 ± 3	1.8 ± 0.4
$t\bar{t}$	2.2 ± 1.1	13 ± 3	0.5 ± 0.5	1.9 ± 0.2	6.8 ± 0.8	0.2 ± 0.1
SM H background	7.1 ± 1.3	5.3 ± 0.8	1.6 ± 0.5	1.9 ± 0.3	1.6 ± 0.2	0.6 ± 0.1
sum of backgrounds	2125 ± 530	513 ± 114	5.4 ± 1.4	160 ± 19	118 ± 9	5.6 ± 0.9
LFV Higgs boson signal	66 ± 18	30 ± 8	2.9 ± 1.1	23 ± 6	13 ± 3	1.2 ± 0.3
data	2147	511	10	180	128	6

The observed and the median expected 95% CL_s upper limits on the $B(H \to \mu\tau)$ for the H mass at 125 GeV are given for each category in Table 7.2. Combining all the channels, an expected upper limit of $B(H \to \mu\tau) < (0.75 \pm 0.38)\%$ is obtained. The observed upper limit is $B(H \to \mu\tau) < 1.51\%$ which is above the expected limit due to an excess of the observed number of events above the background prediction. The fit can then be used to estimate the branching fraction if this excess were to be interpreted as a signal. The best fit values for the branching fractions are given in Table 7.2. The limits and best fit branching fractions are also summarized graphically in Fig. 7.2. The combined categories give a best fit of $B(H \to \mu\tau) = (0.84^{+0.39}_{-0.37})\%$. The combined excess is 2.4 standard deviations which corresponds to a p-value of 0.010 at $M_H = 125$ GeV.

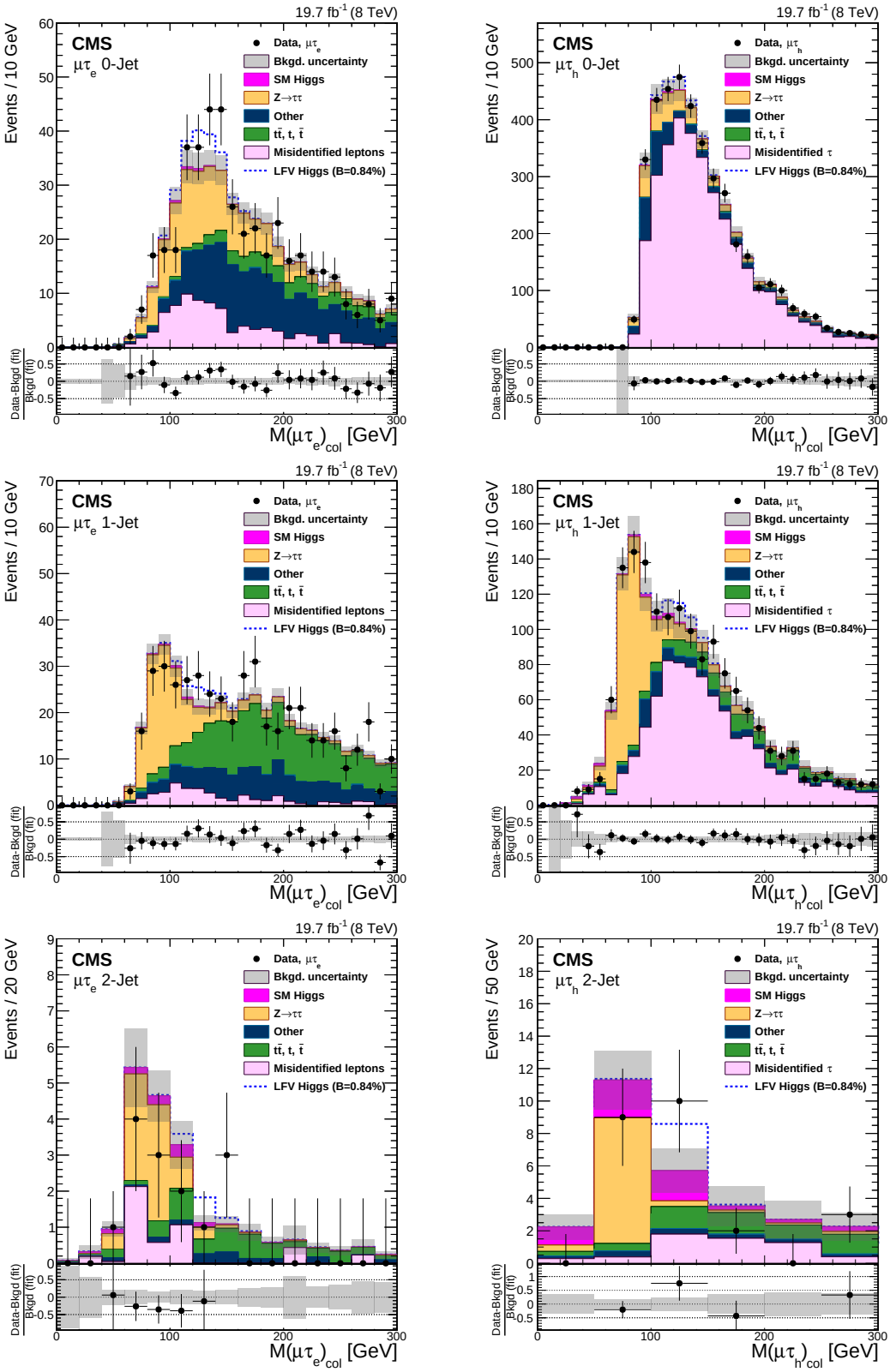

Figure 7.1: Distributions of the collinear mass M_{col} after fitting for signal and background for the LFV $H \to \mu\tau$ candidates in the different channels and categories compared to data. The distribution of the simulated LFV Higgs boson sample is shown for the best fit branching fraction of $B(H \to \mu\tau) = 0.84\%$. The bottom panel in each plot shows the fractional difference between the observed data and the fitted background. Top left: $H \to \mu\tau_e$ 0-jet; top right: $H \to \mu\tau_h$ 0-jet; middle left: $H \to \mu\tau_e$ 1-jet; middle right: $H \to \mu\tau_h$ 1-jet; bottom left: $H \to \mu\tau_e$ 2-jet; bottom right

Table 7.2: The expected upper limits, observed upper limits and best fit values for the branching fractions for different jet categories for the $H \to \mu\tau$ process. The one standard-deviation probability intervals around the expected limits are shown in parentheses.

	0-Jet (%)	1-Jet (%)	2-Jets (%)
Expected Limits			
$\mu\tau_e$	<1.32 (±0.67)	<1.66 (±0.85)	<3.77 (±1.92)
$\mu\tau_h$	<2.34 (±1.19)	<2.07 (±1.06)	<2.31 (±1.18)
$\mu\tau$	<0.75 (±0.38)		
Observed Limits			
$\mu\tau_e$	<2.04	<2.38	<3.84
$\mu\tau_h$	<2.61	<2.22	<3.68
$\mu\tau$	<1.51		
Best Fit Branching Fractions			
$\mu\tau_e$	$0.87^{+0.66}_{-0.62}$	$0.81^{+0.85}_{-0.78}$	$0.05^{+1.58}_{-0.97}$
$\mu\tau_h$	$0.41^{+1.20}_{-1.22}$	$0.21^{+1.03}_{-1.09}$	$1.48^{+1.16}_{-0.93}$
$\mu\tau$	$0.84^{+0.39}_{-0.37}$		

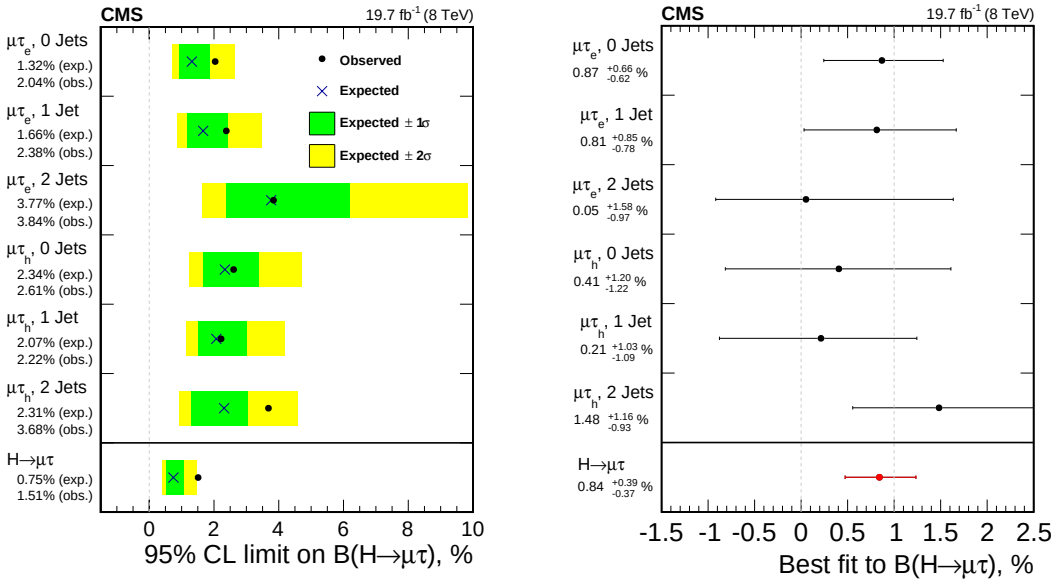

Figure 7.2: Left: 95% CL Upper limits by category for the LFV $H \to \mu\tau$ decays. Right: best fit branching fractions by category.

13 TeV Results

7.2 W+Jets

Detector Unfolding

13 TeV Results

Chapter 8

Conclusions

8.1 Summary

8.2 Future Outlook

Bibliography

[1] Q. R. Ahmad et al. Measurement of the rate of $\nu_e + d \rightarrow p + p + e^-$ interactions produced by ^8B solar neutrinos at the Sudbury Neutrino Observatory. *Phys. Rev. Lett.*, 87:071301, 2001.

[2] Q. R. Ahmad et al. Direct evidence for neutrino flavor transformation from neutral current interactions in the Sudbury Neutrino Observatory. *Phys. Rev. Lett.*, 89:011301, 2002.

[3] Simone Alioli, Paolo Nason, Carlo Oleari, and Emanuele Re. A general framework for implementing NLO calculations in shower Monte Carlo programs: the POWHEG BOX. *JHEP*, 06:043, 2010.

[4] John Allison et al. Geant4 developments and applications. *IEEE Trans. Nucl. Sci.*, 53:270, 2006.

[5] J. Alwall, R. Frederix, S. Frixione, V. Hirschi, F. Maltoni, O. Mattelaer, H. S. Shao, T. Stelzer, P. Torrielli, and M. Zaro. The automated computation of tree-level and next-to-leading order differential cross sections, and their matching to parton shower simulations. *JHEP*, 07:079, 2014.

[6] Nima Arkani-Hamed, Savas Dimopoulos, and G. R. Dvali. The Hierarchy problem and new dimensions at a millimeter. *Phys. Lett.*, B429:263–272, 1998.

[7] Vernon D. Barger and Roger J. N. Phillips. *Collider Physics (Frontiers in Physics)*. Addison Wesley Publishing Company, 1987.

[8] Philip Bevington and D. Keith Robinson. *Data Reduction and Error Analysis for the Physical Sciences*. McGraw-Hill Education, 3rd edition, 7 2002.

[9] G. C. Branco, P. M. Ferreira, L. Lavoura, M. N. Rebelo, Marc Sher, and Joao P. Silva. Theory and phenomenology of two-Higgs-doublet models. *Phys. Rept.*, 516:1–102, 2012.

[10] J. S. Conway. Incorporating Nuisance Parameters in Likelihoods for Multisource Spectra. In *Proceedings, PHYSTAT 2011 Workshop on Statistical Issues Related to Discovery Claims in Search Experiments and Unfolding, CERN,Geneva, Switzerland 17-20 January 2011*, 2011.

[11] Glen Cowan, Kyle Cranmer, Eilam Gross, and Ofer Vitells. Asymptotic formulae for likelihood-based tests of new physics. *Eur. Phys. J.*, C71:1554, 2011. [Erratum: Eur. Phys. J.C73,2501(2013)].

[12] Stefano Frixione, Paolo Nason, and Carlo Oleari. Matching NLO QCD computations with Parton Shower simulations: the POWHEG method. *JHEP*, 11:070, 2007.

[13] Y. Fukuda et al. Evidence for oscillation of atmospheric neutrinos. *Phys. Rev. Lett.*, 81:1562–1567, 1998.

[14] F. Halzen and Alan D. Martin. Quarks and leptons: An introductory course in modern particle physics. 1984. New York, Usa: Wiley (1984) 396p.

[15] Roni Harnik, Joachim Kopp, and Jure Zupan. Flavor Violating Higgs Decays. *JHEP*, 03:026, 2013.

[16] Paolo Nason. A New method for combining NLO QCD with shower Monte Carlo algorithms. *JHEP*, 11:040, 2004.

[17] K. A. Olive et al. Review of Particle Physics. *Chin. Phys.*, C38:090001, 2014.

[18] Lisa Randall and Raman Sundrum. A Large mass hierarchy from a small extra dimension. *Phys. Rev. Lett.*, 83:3370–3373, 1999.

[19] A L Read. Modified frequentist analysis of search results (the CL_s method). (CERN-OPEN-2000-205), 2000.

[20] Torbjrn Sjstrand, Stefan Ask, Jesper R. Christiansen, Richard Corke, Nishita Desai, Philip Ilten, Stephen Mrenna, Stefan Prestel, Christine O. Rasmussen, and Peter Z. Skands. An Introduction to PYTHIA 8.2. *Comput. Phys. Commun.*, 191:159–177, 2015.

[21] A. Wald. *Tests of Statistical Hypotheses Concerning Several Parameters when the Number of Observations is Large*. American Mathematical Society, 1943.

[22] Zbigniew Was. TAUOLA for simulation of tau decay and production: perspectives for precision low energy and LHC applications. *Nucl. Phys. Proc. Suppl.*, 218:249–255, 2011.